Discovery of a new type of magnetic order on pyrochlore spinels

GiBaik Sim* and SungBin Lee†
Department of Physics, Korea Advanced Institute of Science and Technology, Daejeon 305-701, Korea

(Received 14 March 2018; revised manuscript received 20 May 2018; published 23 July 2018)

Frustration in a spin system can give rise to unique ordered states and as a consequence several physical phenomena are expected, such as multiferroics, high temperature superconductors, and anomalous Hall effect. Here we report the "new magnetic orders" induced by anisotropic spin exchanges on pyrochlore spinels as the interplay of spin-orbit coupling and geometrical frustration. Due to complicated superexchange paths of B-site spinels, we claim that anisotropic interaction between next-nearest neighbors play an important role. Based on the systematic studies of the spin model, we argue that several classical spin states can be explored in spinel systems; local XY state, all-in all-out state, Palmer-Chalker state, and coplanar spiral state. In addition, we reveal new types of magnetic phases with finite ordering wave vectors, labeled as *octagonal (prism)* state and *(distorted) cubic* states. When the *octagonal prism* state is stabilized, nonzero scalar spin chirality induces alternating net current in addition to finite orbital current and orbital magnetization even in Mott insulators. Finally, we also discuss the relevance of *distorted cubic* state to the magnetic order of spinel compound $GeCo_2O_4$.

DOI: 10.1103/PhysRevB.98.014423

Magnetic frustration originates from competing interactions between different spin exchanges. Despite the simple spin interactions such as Heisenberg or Ising type, lattice geometries can give rise to frustration, often termed as geometrical frustration [1,2]. Apart from geometrical frustration, anisotropic spin exchanges can also give rise to frustration due to competing interactions [3–6]. In general, such anisotropic spin exchanges are expected for a spin-orbit coupled system described by the total angular momentum J. When anisotropic spin exchanges meet geometrical frustration, exotic magnetism emerges in Mott insulators.

Magnetic properties of the B-site spinel compounds (AB_2X_4) own such interplay forming a corner shared tetrahedra, pyrochlore lattice structure [7–9]. Focusing on pyrochlore lattice structure, one can derive the most generic spin model on symmetry grounds and indeed such a generic spin model for nearest-neighbor interactions has been studied. Especially for rare-earth pyrochlore magnets ($A_2B_2O_7$), A site rare-earth ions also form a pyrochlore lattice and their partially filled $4f$ electrons can give rise to non-negligible anisotropic spin exchanges between nearest neighbors [10–13]. However, the situation in B-site spinels with $3d$-$5d$ magnetic ions is quite different from the case of rare-earth pyrochlores. In spinels, the superexchange paths induce anisotropic exchanges between next-nearest neighbor to play an important role, thus the spin model for B-site spinel compounds is significantly distinct from ones studied before and one could expect new types of magnetic orderings.

In this paper we study the frustrated spin model on a pyrochlore lattice and find new magnetic phases and their unique properties. Focusing on spin-orbit coupled B-site spinels, we write down the spin exchange Hamiltonian derived from the Hubbard model with a pseudospin $j_{\text{eff}} = 1/2$ Kramers doublet. Considering superexchange paths for neighbors between B-site magnetic ions, we claim that next-nearest neighbor anisotropic exchanges generally dominate in determining the magnetic ground states. Within a classical spin approach, we employ the Luttinger-Tisza method [14] and iterative minimization method [15] (with system size up to $12 \times 12 \times 12$) to investigate the magnetic phase diagram. Our key result is the discovery of *new magnetic orderings* described with finite ordering wave vectors $\boldsymbol{Q}$; *octagonal (prism)* state and *(distorted) cubic* states. We also argue their interesting consequences like orbital currents and relevance to spinel compounds $GeCo_2O_4$. Another main issue is that such a spin model of B-site spinels can also lead to many interesting magnetic phases with $\boldsymbol{Q} = 0$ ordering; local XY, all-in all-out, and Palmer-Chalker states [16–18]. We note that these $\boldsymbol{Q} = 0$ phases originate from anisotropic spin exchanges between next-nearest neighbors, even in the absence of nearest-neighbor interactions or long range dipolar interactions.

I. MODEL

When the B site of spinel is occupied by transition metal ions with partially filled $3d$-$5d$ orbitals, cubic crystal symmetry splits d orbitals into t_{2g} and e_g and spin-orbit coupling further splits t_{2g} orbitals into $j_{\text{eff}} = 3/2$ quadruplet and $j_{\text{eff}} = 1/2$ doublet described by isospin configuration. Within pseudospin $j_{\text{eff}} = 1/2$ doublet, one writes down the simple Hubbard model

$$\mathcal{H} = \sum_{ij,\alpha\beta} c^{\dagger}_{i\alpha}(t_{ij}\mathbb{I} + i\mathbf{d}_{ij}\cdot\boldsymbol{\sigma})_{\alpha\beta}c_{j\beta} + U\sum_i n_{i\uparrow}n_{j\downarrow}, \quad (1)$$

where the first term represents electron hopping within pseudospin-1/2 manifold between sites i and j (which includes both spin independent and dependent hoppings), and the second term represents electron interaction. For B-site spinels with $j_{\text{eff}} = 1/2$ doublet, the nearest-neighbor (NN)

*gbsim1992@kaist.ac.kr
†sungbin@kaist.ac.kr

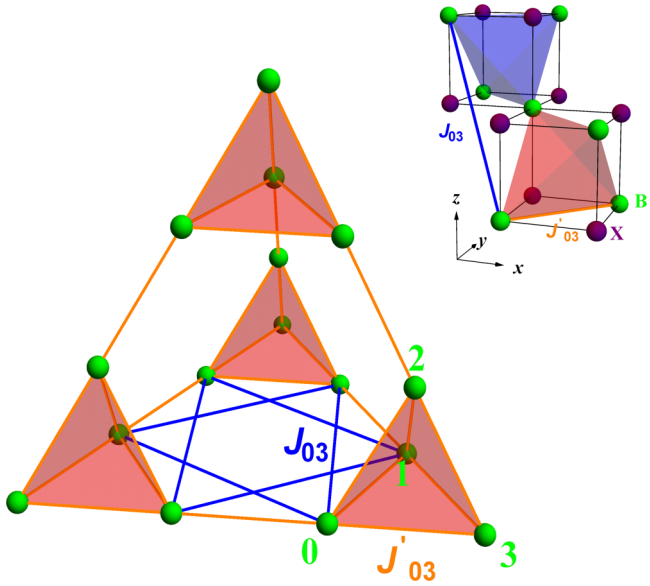

FIG. 1. Pyrochlore lattice structure and connectivity between nearest-neighbor sites (NN) and next-nearest-neighbor sites (NNN). To see the connectivity between NNNs, a super tetrahedron is shown which consists of four tetrahedra. Each face of the super tetrahedron forms a hexagon connected by NNs (marked as solid lines with orange color). In every hexagon, two triangles (solid lines with blue color) exhibit the connectivity between NNNs. The inset shows a schematic picture of the B-site spinel structure only focusing onto X ions and B ions. See the main contents for a detailed explanation.

interactions via X mediated superexchanges completely vanish. However, the next-nearest-neighbor (NNN) interactions via X-A-X mediated superexchanges generate both finite spin dependent and independent terms (i.e., $t_{ij} \neq 0$ and $\mathbf{d}_{ij} \neq 0$ between the NNN sites i and j). Furthermore, it turns out that the magnitude of $|\mathbf{d}_{ij}|/t_{ij}$ is quite large, indicating the importance of spin dependent hopping between NNNs. (See the Supplemental Material [19] for details.) In the Mott insulating regime, therefore, we derive the following spin Hamiltonian with NNs and NNNs at large U:

$$\mathcal{H} = \sum_{\langle ij \rangle} J'^{\alpha\beta}_{ij}(\Omega) S^{\alpha}_{i} S^{\beta}_{j} + \sum_{\langle\langle ij \rangle\rangle} J^{\alpha\beta}_{ij}(\phi,\theta) S^{\alpha}_{i} S^{\beta}_{j}, \qquad (2)$$

where $\langle ij \rangle$ and $\langle\langle ij \rangle\rangle$ indicates the nearest-neighbor (NN) and next-nearest-neighbor (NNN) interactions between i site and j site, J' and J characterize exchange coupling between NNs and NNNs, respectively. On symmetry grounds, the interactions between NNs only require one dimensionless parameters $\Omega = \tan^{-1}(\pm|\mathbf{d}_{ij}|/t_{ij})$ with $\langle ij \rangle$, while the interactions between NNNs require two parameters ϕ and θ; ϕ which parametrizes the unit vector $\hat{\mathbf{d}}_{ij}$ lying on the plane perpendicular to the twofold rotation axis and $\theta = \tan^{-1}(\pm|\mathbf{d}_{ij}|/t_{ij})$ with $\langle\langle ij \rangle\rangle$. (A detailed derivation is explained in the Supplemental Material [19].) For clarification, Eq. (3) exemplifies $\mathbf{J}'_{ab}(\Omega)$ and $\mathbf{J}_{cd}(\phi,\theta)$ for a given bond, marked as J_{03} and J'_{03} respectively in Fig. 1. (See the Supplemental Material [19] for the detail form of j'_n and j_n in terms of Ω and (ϕ,θ), respectively.)

$$\mathbf{J}'_{03}(\Omega) = \begin{pmatrix} j'_2 & j'_3 & j'_4 \\ j'_3 & j'_2 & j'_4 \\ -j'_4 & -j'_4 & j'_1 \end{pmatrix}, \quad \mathbf{J}_{03}(\phi,\theta) = \begin{pmatrix} j_6 & j_3 & -j_2 \\ j_5 & j_6 & -j_4 \\ j_4 & j_2 & j_1 \end{pmatrix}. \qquad (3)$$

The lattice structure of pyrochlores especially for the connectivity between NNNs is shown in Fig. 1. The super tetrahedron includes four tetrahedra (colored in red) and each tetrahedron is made by four sublattices (green spheres). Here the NNs are marked by orange solid lines. In the super tetrahedron structure, each face consists of a hexagon formed by three tetrahedra. In a hexagon (we focus on one at the bottom of the super tetrahedron), the NNNs connect different sublattices forming two triangles, marked as blue solid lines in Fig. 1. In total, each sublattice has 6 NNs and 12 NNNs in a pyrochlore lattice.

II. MAGNETIC PHASE DIAGRAM

Taking into account the previous argument of superexchange paths, we start from the general spin model for NNNs, i.e., a finite $J^{\alpha\beta}_{ij}(\phi,\theta)$ with $J'^{\alpha\beta}_{ij}(\Omega) = 0$ first and then consider the stabilities of each phase with finite NN interactions. Figure 2 shows the phase diagram with two dimensionless parameters ϕ and θ. It is worth to note that any point with a given parameter (ϕ,θ) is identical to the point with

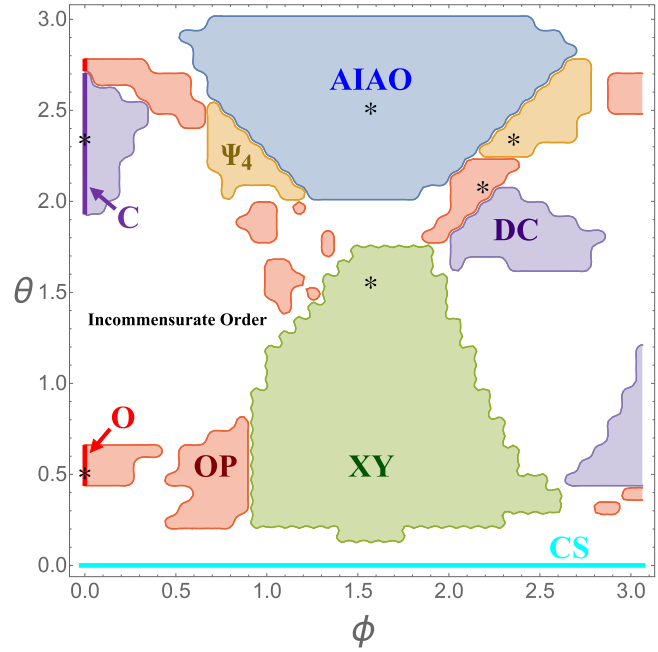

FIG. 2. Phase diagram of magnetic ordering as functions of ϕ and θ: Green, blue, and orange regions denote local XY phase (XY), all-in all-out phase (AIAO), and Palmer-Chalker phase (Ψ_4), respectively, which all belong to $Q = 0$ ordering. Red and purple regions represent octagonal prism phase (OP) and distorted cubic phase (DC), which all belong to noncoplanar ordering with finite Q's. Thick red, purple, and cyan lines mark octagonal (O), cubic (C), and coplanar spiral (CS) phases. See the main text for a detailed description.

TABLE I. Summary of classical magnetic ground states of Eq. (2): For given ground states, coplanarity and ordering wave vector $\boldsymbol{Q}$ are described and the stability of each phase (at $*$ points in Fig. 2) in the presence of nearest-neighbor Heisenberg interaction J_1 is shown in the last column. (Negative J_1 is for ferromagnet.)

Ground states	Coplanarity	$\boldsymbol{Q}$	$J_1(*)$
Coplanar spiral (CS)	Yes	$(\frac{4\pi}{3}00)$	–
Local XY (XY)	No	(000)	$-1.8,\infty$
All-in all-out (AIAO)	No	(000)	$-0.3,\infty$
Palmer-Chalker (Ψ_4)	Yes	(000)	$-1.6,\infty$
Octagonal (O)	Yes	$(2\pi\pi 0)$	$-2.6,0.2$
Octagonal prism (OP)	No	$(2\pi\pi 0)$	$-0.1,0.9$
Cubic (C)	No	$(\pi\pi\pi)$	–
Distorted cubic (DC)	No	$(\pi\pi\pi)$	$-0.7,10$

$[\phi + m\pi,(-1)^m\theta + n\pi]$ where m and n are arbitrary integers. Thus, we plot the phase diagram within the parameter ranges $\phi \in [0,\pi)$ and $\theta \in [0,\pi)$.

In the colored regions, we have found magnetic phases with commensurate ordering wave vectors where both Luttinger-Tisza and iterative minimization agrees with each other. (Explanation of each method is given in the Supplemental Material [19].) However, in the rest of parameter space, we have only found incommensurate ordering wave vectors within Luttinger-Tisza approximation. To check the stability of each phase, one specific parameter at each phase is chosen (marked as $*$ in Fig. 2) and we investigate the phase robustness in the presence of the nearest-neighbor Heisenberg interaction J_1. Table I shows the summary of magnetic ground states we have found in our model.

Coplanar phases with $\boldsymbol{Q} \neq 0$*:* At $\theta = 0$ our model becomes a simple antiferromagnetic (AF) Heisenberg model of NNNs. In this limit, the model has been already investigated and its magnetic ground state is described by coplanar spiral phase (marked as CS in Fig. 2.) with an ordering wave vector $\boldsymbol{Q} = (\frac{4\pi}{3},0,0)$ [20]. Unlike the case of AF interaction between NNs where the system possess extensive degeneracy of magnetic ground states, AF interaction between NNNs favors specific coplanar spiral state with a finite $\boldsymbol{Q}$.

When $(\phi = 0,0.45 \lesssim \theta \lesssim 0.65)$ or $(\phi = 0,2.73 \lesssim \theta \lesssim 2.77)$ marked as a thick red colored region in Fig. 2, there is another coplanar phase which is described with an ordering wave vector at high symmetric W point [see Fig. 3(c)]. In this phase, spins at sublattice 0 and 2 [colored blue in Fig. 3(a)] point four different directions, whereas at sublattices 1 and 3 [colored green in Fig. 3(a)], spins point another four different directions. Since spins point all eight different directions in total, we label this phase as *octagonal* (O) phase. The spin configuration at a sublattice a is $\boldsymbol{S}_a = \boldsymbol{\Psi}_a \exp(i\boldsymbol{Q}\cdot\boldsymbol{R}) + \text{c.c.}$ with $\boldsymbol{\Psi}_a = (fe^{-i\beta(-1)^a},0,-ife^{i\beta(-1)^a})$, (f,β) are functions of the parameter θ and $\boldsymbol{Q} = (2\pi,\pi,0)$. (Illustration of spin configuration is given in the Supplemental Material [19].)

Magnetic phases with $\boldsymbol{Q} = 0$*:* As we tune parameters ϕ and θ, our model shows three different types of magnetic phases without enlarging unit cell $\boldsymbol{Q} = 0$; all-in all-out phase (AIAO), local XY phase (XY), and Palmer-Chalker phase (Ψ_4). All these phases belong to the degenerate ground state manifolds of AF Heisenberg interaction between NNs, satisfying the sum of four spins for every tetrahedron to be zero. Thus, these phases are stable even in the limit of $J_1 \to \infty$ as shown in Table I.

In blue colored region in Fig. 2 *all-in all-out* phase is stabilized. With a given local coordinate at each sublattice, all-in all-out phase is described by all four spins in a unit cell aligned on their local $\hat{z}$ or $-\hat{z}$ axes, having twofold degeneracy. (See the Supplemental Material [19] for a description of local coordinates and spin configuration.)

In *local XY phase*, on the other hand, each spin lies in its local xy plane, having the same azimuthal angle $\varphi_a \equiv \varphi$. (See the green colored region in Fig. 2.) φ_a is measured within local xy plane starting from local x axis for each sublattice a. In this phase, one can freely choose $\varphi \in [0,2\pi)$ thus $U(1)$ symmetry is present at a mean field level. (See the Supplemental Material [19] for illustration of spin configuration.) There is possible quantum or thermal order by disorder in this phase, having *pseudo*-Goldstone mode with little gap at low temperature. Since this local XY phase is stabilized by anisotropic spin interactions between NNNs, it may choose different ordered phase due to fluctuations compared to the case studied in Refs. [21–23] and further detailed studies are required in the future.

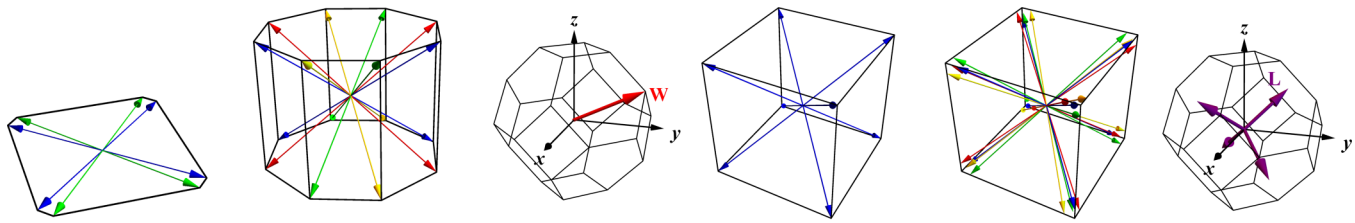

(a) **COP** of **O** (b) **COP** of **OP** (c) $\boldsymbol{Q}$ of **O** or **OP** (d) **COP** of **C** (e) **COP** of **DC** (f) $\boldsymbol{Q}$ of **C** or **DC**

FIG. 3. Common origin plots (COP) and magnetic ordering wave vectors $\boldsymbol{Q}$ of *octagonal (prism)* phase and *(distorted) cubic* phase: (a) *Octagonal* (O) phase—Spins point eight different directions on a plane. Spin directions at sublattices 0 and 2 (1 and 3) are identical as colored in blue (green). (b) *Octagonal prism* (OP) phase—Spins at each sublattice form a plane and the planes are distinct for sublattices, forming a shape of an octagonal prism. Four distinct colors indicate the spin directions in different sublattices. (c) $\boldsymbol{Q}$ of O and OP phase—Magnetic ordering wave vector is located at W points shown in the first Brillouin zone. (d) *Cubic* (C) phase—Spins point all eight different directions forming a cubic structure. At every sublattice, spins are pointing every eight vertices of cube. (e) *Distorted cubic* (DC) phase—Spins point all 32 different directions resulting in distortion of perfect cube. At every sublattice, spins are pointing every eight vertices of one rhombohedron. (f) $\boldsymbol{Q}$ of C and DC phase—Both C and DC phases are described by ordering wave vectors located at high symmetric L points. More detailed explanation is given in the main text.

The Palmer-Chalker state (or equivalently referred as Ψ_4 state) is stabilized in the orange colored region in Fig. 2 [18,24]. It is described by the following three different sets of azimuthal angles φ_a for sublattices a ($a \in 0$, 1, 2, and 3), and their time reversal symmetric partners (six different configurations in total): $(\varphi_0 = \varphi_1 = \frac{\pi}{2}, \varphi_2 = \varphi_3 = \frac{3\pi}{2})$, $(\varphi_0 = \varphi_2 = \frac{7\pi}{6}, \varphi_1 = \varphi_3 = \frac{\pi}{6})$, $(\varphi_0 = \varphi_3 = \frac{11\pi}{6}, \varphi_1 = \varphi_2 = \frac{5\pi}{6})$ [23]. (Image of spin configuration is given in the Supplemental Material [19].) It is remarkable that this phase is stabilized by anisotropic NNN exchanges even without long range dipolar interaction or thermal/quantum fluctuations.

Noncoplanar phases with $Q \neq 0$*:* Many noncoplanar magnetic orderings give fertile grounds where interesting phenomena emerge, such as orbital currents and anomalous Hall effect induced by nonzero spin chirality [25,26]. Although there exist earlier studies related to noncoplanar phases with $\boldsymbol{Q} \neq 0$ in pyrochlores, those are stabilized only as metastable phases or due to itinerant electrons [27,28]. In our model, we find two new types of magnetic orderings as ground states: *octagonal prism* phase and *(distorted) cubic* phase. In Fig. 2, both red or purple regions are where such noncoplanar states are stabilized.

Octagonal prism phase (OP): This noncoplanar phase is described by the ordering wave vector W same as coplanar *octagonal* phase but spins point 16 different directions forming a shape of an octagonal prism as shown in Fig. 3(b). Thus we refer it as *octagonal prism* phase. In this phase, the spins at each sublattice still form a coplanar state but their planes are distinct by sublattices. Common origin plot of all spin configurations is shown in Fig. 3(b). Blue, green, red, and yellow colors indicate the spin directions in each sublattice. The magnetic unit cell is quadrupled where spins at each sublattice align on a certain plane but the planes are distinct for different sublattices. In detail, spin configuration at a sublattice a is parametrized as $\boldsymbol{S}_a = \boldsymbol{\Psi}_a \exp(i\boldsymbol{Q}\cdot\boldsymbol{R}) + \text{c.c.}$ with $\boldsymbol{\Psi}_a = (fe^{-i\beta(-1)^a}, ge^{-\frac{i\pi}{4}(2a-1)}, -ife^{i\beta(-1)^a})$, (f,g,β) are functions of (ϕ,θ) and $\boldsymbol{Q} = (2\pi,\pi,0)$. (See the Supplemental Material [19] for illustration of spin configuration.)

In this phase, noncoplanar spin orderings can give rise to net scalar spin chirality on each triangle connected by the NNNs as shown in Fig. 4. Having a finite spin chirality, the orbital current is generally induced even in the Mott insulating phase [26,29]. Figure 4 shows the existence of net scalar spin chirality on each triangle formed by three sites i, j, and k, $\chi_{ijk} = \mathbf{S}_i \cdot (\mathbf{S}_j \times \mathbf{S}_k)$ on (111) plane. Triangles with blue (red) color exhibit positive (negative) spin chirality χ_{ijk} where sites i, j, and k are taken in counterclockwise direction, and the relative magnitudes of χ_{ijk} are represented by bond thickness. At a given bond connected by two sites i and j, the third order of perturbation theory at $O(t^3/U^2)$ induces the net current proportional to $\mathbf{I}_{ij,k} \sim \hat{\mathbf{r}}_{ij}\chi_{ijk}$, where $\hat{\mathbf{r}}_{ij}$ is the unit vector from site i to site j [26]. This orbital current is like the persistent current in superconducting phase and it furthermore leads to the finite orbital magnetic moment $\mathbf{L}_{ijk} \propto \chi_{ijk}\hat{\mathbf{z}}$ where $\hat{\mathbf{z}}$ is normal to the plane of the triangle. As seen in Fig. 4, the orbital current induced by net scalar spin chirality also makes the special current channel along $\pm[1\bar{2}1]$ directions (blue or red colored thick lines) on (111) plane. Experimental observation of such spatially varying current channel will be the challenging future work.

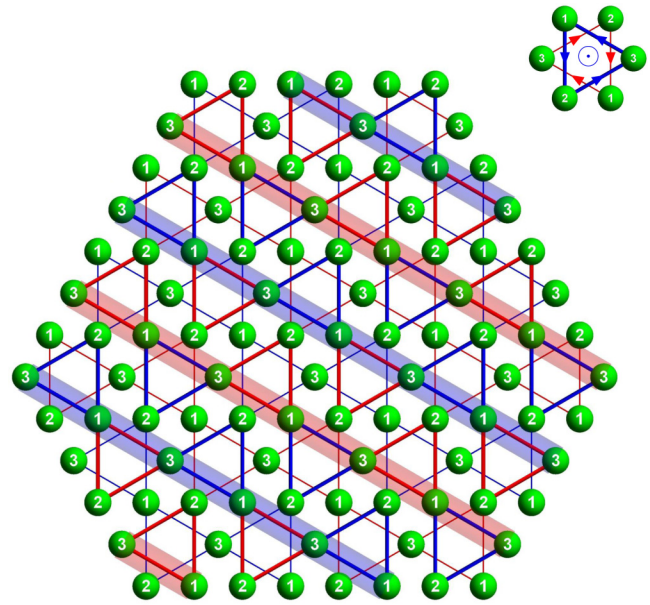

FIG. 4. Scalar spin chirality at each triangle on (111) plane of pyrochlores. Blue (red) colored triangles exhibit positive (negative) chirality and bond thickness represents its magnitude. The thick lines colored by blue and red are the direction $\pm[1\bar{2}1]$ of current channel induced by scalar spin chirality. See the main text for more explanation.

(Distorted) cubic phase (C or DC): At the region marked with thick purple color in Fig. 2, the ordering wave vectors are at high symmetric L points [see Fig. 3(f)] and common origin plot of spin orderings is shown in Fig. 3(d). In this phase, spins at every sublattice point eight different directions forming a cubic structure and spin orderings at different sublattices are all identical consisting of the same cube. Thus we label it as *cubic* (C) phase. In detail, spin configuration at each sublattice is represented as follows:

$$\boldsymbol{S}_a = \frac{e^{i\gamma_a}}{\sqrt{3}}(\hat{\boldsymbol{x}}e^{i\boldsymbol{Q}_a\cdot\boldsymbol{R}} + \hat{\boldsymbol{y}}e^{i\boldsymbol{Q}'_a\cdot\boldsymbol{R}} + \hat{\boldsymbol{z}}e^{i\boldsymbol{Q}''_a\cdot\boldsymbol{R}}). \tag{4}$$

Here $(\boldsymbol{Q}_a, \boldsymbol{Q}'_a, \boldsymbol{Q}''_a, \gamma_a)$ are three different ordering wave vectors $\boldsymbol{Q}_a$, $\boldsymbol{Q}'_a$, $\boldsymbol{Q}''_a$ and relative phase γ_a at a sublattice a. For sublattice $a = 0$, 1, 2, and 3, $(\boldsymbol{q}_2,\boldsymbol{q}_3,\boldsymbol{q}_4,0)$, $(\boldsymbol{q}_1,\boldsymbol{q}_4,\boldsymbol{q}_3,\pi)$, $(\boldsymbol{q}_4,\boldsymbol{q}_1,\boldsymbol{q}_2,\pi)$, and $(\boldsymbol{q}_3,\boldsymbol{q}_2,\boldsymbol{q}_1,\pi)$, respectively, where ordering wave vectors $\boldsymbol{q}_s$ are symmetry related distinct L points defined by $\boldsymbol{q}_1 = (\pi,\pi,\pi)$, $\boldsymbol{q}_2 = (-\pi,\pi,\pi)$, $\boldsymbol{q}_3 = (\pi,-\pi,\pi)$, and $\boldsymbol{q}_4 = (\pi,\pi,-\pi)$. (See the Supplemental Material [19] for image of spin configuration.) As described in Eq. (4), spin configuration at every sublattice is described by three distinct ordering wave vectors and each ordering wave vector describes x, y, or z components of spin for a particular sublattice. One can easily understand the magnetic unit cell size is octupled compared to the original fcc lattice unit cell. With an infinitesimal J_1, the cubic phase undergoes the distorted cubic phase, discussed in the following paragraph.

The parameter change of ϕ from 0 makes small deviation of spin direction from the vertices of cube, resulting in

distorted cubic phase, shown in the parameter space colored with purple in the phase diagram Fig. 2. In this phase, spins at each sublattice point eight different directions forming a rhombohedron. For instance, the cubic structure formed by the common origin plot of spins at sublattice 0 [colored in blue in Fig. 3(e)] goes through the rhombohedral distortion along [111] direction. Similarly, the cubic structure formed by the spins at different sublattices also goes through the rhombohedral distortion along their local $\hat{z}$ axis. Similar to the cubic phase, magnetic ordering wave vectors are at high symmetric L points with octupled magnetic unit cell. This distorted cubic phase is remarkably stable against the AF NN exchanges. It can be understood by the fact that the net sum of spins for each tetrahedron is quite small in this phase, thus it is stable even in the presence of large $J_1 > 0$.

In these phases, one can also expect the finite scalar spin chirality as we discussed in the case of the octagonal prism state and it could generate the orbital current and orbital magnetization even in Mott insulators. However, unlike the case of octagonal prism state, we found that the induced orbital current in these phases does not open special channels for uniform current flow along certain directions.

Application to spinel compound $GeCo_2O_4$*:* In spinel compounds $GeCo_2O_4$, A-site Ge^{4+} is nonmagnetic and B-site Co^{2+} ions have partially filled d orbitals with $3d^7$ surrounded by octahedrally coordinated oxygens. The Co ions realize high spin state with $S = 3/2$ having five electrons occupied in t_{2g} orbitals and two electrons occupied in e_g orbitals. The magnetic ordering occurs at $T_N = 21$ K, distinct from structural transition at $T_S = 16$ K and the neutron powder diffraction experiments exhibit the Bragg peak at $\pi(1,1,1)$ due to magnetic reflection [30–33]. In addition, the magnetic ordering is known to be noncollinear based on magnetoelectric signature in this material and thus such ordering could be relevant to the distorted cubic phase we have studied [34]. For more argument, however, future experiments will be required to analyze the exact magnetic ground state.

III. DISCUSSION

In this paper we have studied the spin model of pyrochlore spinels. Motivated by geometrical frustration in pyrochlores, we further explored the role of anisotropic spin interactions. Especially focusing on the spin-orbit coupled system, we derived the spin exchanges based on psudospin $j_{\text{eff}} = 1/2$ Hubbard model. It turns out that the anisotropic spin exchanges between next-nearest neighbors play a dominant role in determining magnetic ground state due to complicated superexchange paths in pyrochlore spinels. It is notable that *local XY*, *all-in all-out*, and *Palmer-Chalker* phases described by zero ordering wave vectors also emerge purely by anisotropic exchanges between next-nearest neighbor even in the absence of nearest-neighbor interactions. More remarkably, we have newly discovered *noncoplanar magnetic orderings* described by finite ordering wave vectors; *octagonal prism* phase and *(distorted) cubic* phase. These noncoplanar states can give rise to unique properties in the Mott insulators, such as orbital current and orbital magnetization induced by scalar spin chirality. One of the pronounced effect in the octagonal prism state is an alternating net current along certain direction. In addition, we also discuss the distorted cubic phase may help understanding the magnetic order in $GeCo_2O_4$ spinel compounds. Our theoretical prediction of exotic magnetic states opens a new search of pyrochlore spinel materials with spin-orbit coupling, and guide further theoretical and experimental studies.

ACKNOWLEDGMENTS

We would like to thank L. Balents, H. Takagi, R. Seshadri, and S. Ji for useful discussions and comments. Hospitality at APCTP during the program "Asia Pacific Workshop on Quantum Magnetism" is kindly acknowledged. S.B.L thanks the hospitality at the Physics Department of University of California, San Diego. G.B.S and S.B.L are supported by the KAIST startup funding and National Research Foundation Grant (NRF-2017R1A2B4008097).

[1] A. Ramirez, Annu. Rev. Mater. Sci. **24**, 453 (1994).
[2] L. Balents, Nature (London) **464**, 199 (2010).
[3] I. Dzyaloshinsky, J. Phys. Chem. Solids **4**, 241 (1958).
[4] T. Moriya, Phys. Rev. **120**, 91 (1960).
[5] G. Chen and L. Balents, Phys. Rev. B **78**, 094403 (2008).
[6] G. Jackeli and G. Khaliullin, Phys. Rev. Lett. **102**, 017205 (2009).
[7] E. Bertaut, V. Van Qui, R. Pauthenet, and A. Murasik, J. Phys. **25**, 516 (1964).
[8] S.-H. Lee, H. Takagi, D. Louca, M. Matsuda, S. Ji, H. Ueda, Y. Ueda, T. Katsufuji, J.-H. Chung, S. Park *et al.*, J. Phys. Soc. Jpn. **79**, 011004 (2010).
[9] H. Takagi and S. Niitaka, Highly frustrated magnetism in spinels, in *Introduction to Frustrated Magnetism: Materials, Experiments, Theory*, edited by C. Lacroix, P. Mendels, and F. Mila (Springer, Berlin, 2011), pp. 155–175.
[10] J. S. Gardner, M. J. Gingras, and J. E. Greedan, Rev. Mod. Phys. **82**, 53 (2010).
[11] J. Thompson, P. McClarty, D. Prabhakaran, I. Cabrera, T. Guidi, and R. Coldea, Phys. Rev. Lett. **119**, 057203 (2017).
[12] K. A. Ross, L. Savary, B. D. Gaulin, and L. Balents, Phys. Rev. X **1**, 021002 (2011).
[13] S. B. Lee, S. Onoda, and L. Balents, Phys. Rev. B **86**, 104412 (2012).
[14] J. Luttinger and L. Tisza, Phys. Rev. **70**, 954 (1946).
[15] Y. Tymoshenko, Y. Onykiienko, T. Müller, R. Thomale, S. Rachel, A. Cameron, P. Portnichenko, D. Efremov, V. Tsurkan, D. Abernathy *et al.*, Phys. Rev. X **7**, 041049 (2017).
[16] S. T. Bramwell and M. J. Gingras, Science **294**, 1495 (2001).
[17] M. J. Gingras and P. A. McClarty, Rep. Prog. Phys. **77**, 056501 (2014).
[18] S. E. Palmer and J. T. Chalker, Phys. Rev. B **62**, 488 (2000).

[19] See Supplemental Material at http://link.aps.org/supplemental/10.1103/PhysRevB.98.014423 for derivation of the Slater-Koster parametrization, explanation of Luttinger-Tisza and iterative minimization methods, derivation of generic spin Hamiltonian on symmetry grounds, and illustration of spin configurations.
[20] M. F. Lapa and C. L. Henley, arXiv:1210.6810.
[21] L. Savary, K. A. Ross, B. D. Gaulin, J. P. C. Ruff, and L. Balents, Phys. Rev. Lett. **109**, 167201 (2012).
[22] A. W. C. Wong, Z. Hao, and M. J. P. Gingras, Phys. Rev. B **88**, 144402 (2013).
[23] P. A. McClarty, P. Stasiak, and M. J. P. Gingras, Phys. Rev. B **89**, 024425 (2014).
[24] A. Poole, A. Wills, and E. Lelievre-Berna, J. Phys.: Condens. Matter **19**, 452201 (2007).
[25] Y. Taguchi, Y. Oohara, H. Yoshizawa, N. Nagaosa, and Y. Tokura, Science **291**, 2573 (2001).
[26] L. N. Bulaevskii, C. D. Batista, M. V. Mostovoy, and D. I. Khomskii, Phys. Rev. B **78**, 024402 (2008).
[27] G.-W. Chern, Phys. Rev. Lett. **105**, 226403 (2010).
[28] T. Okubo, T. H. Nguyen, and H. Kawamura, Phys. Rev. B **84**, 144432 (2011).
[29] R. Shindou and N. Nagaosa, Phys. Rev. Lett. **87**, 116801 (2001).
[30] S. Diaz, S. de Brion, G. Chouteau, B. Canals, V. Simonet, and P. Strobel, Phys. Rev. B **74**, 092404 (2006).
[31] M. Matsuda, T. Hoshi, H. Aruga Katori, M. Kosaka, and H. Takagi, J. Phys. Soc. Jpn. **80**, 034708 (2011).
[32] X. Fabrèges, E. Ressouche, F. Duc, S. de Brion, M. Amara, C. Detlefs, L. Paolasini, E. Suard, L.-P. Regnault, B. Canals *et al.*, Phys. Rev. B **95**, 014428 (2017).
[33] P. T. Barton, M. C. Kemei, M. W. Gaultois, S. L. Moffitt, L. E. Darago, R. Seshadri, M. R. Suchomel, and B. C. Melot, Phys. Rev. B **90**, 064105 (2014).
[34] R. Seshadri (private communication).